Analysis of two-phase pressure drop fluctuations during micro-channel flow boiling

Yuan Wang, Khellil Sefiane, Zhengguo Wang, Souad Harmand

Analysis of Two-Phase Pressure Drop Fluctuations during Micro-channel Flow Boiling

Yuan WANG[a], Khellil SEFIANE[b], Zhen-guo WANG[a], Souad Harmand[c]

[a.]Science and Technology on Scramjet Laboratory, National University of Defense Technology, Hunan, Changsha 410073, People's Republic of China

[b.]School of Engineering, University of Edinburgh, The King's Buildings, Mayfield Road, Edinburgh, EH9 3JL, UK

[c]UVHC, TEMPO, F-59313, Universite Valenciennes, France

Abstract

Two-phase pressure drop fluctuations during flow boiling in single micro-channel were experimentally investigated. Degassed FC-72 was tested in micro-channels with a hydraulic diameters of 571 μm, 762 μm and 1454 μm (the aspect ratio (W_{in}/d_{in}) is 20, 20 and 10) at liquid mass fluxes of 11.2 kg·m^{-2}·s^{-1}, 22.4 kg·m^{-2}·s^{-1} and 44.8 kg·m^{-2}·s^{-1} and heat fluxes of 0-18.31 kW·m^{-2}. Flow instabilities were analyzed based on the two-phase pressure drop, synchronous visualization results and thermographic measurements of the channel surface temperature profiles. Low-frequency high-amplitude fluctuation and high-frequency low-amplitude fluctuation are identified, the main causes of which were found to be the periodic reverse and rewetting flow and the vapour slug cluster passage respectively. The analysis based on a non-dimensional parameter K_1 helps to better understand the dominant influence on the liquid-vapour interface movement during flow boiling. Effects of heat flux, mass flux and channel hydraulic diameter on the pressure drop fluctuation were discussed. Besides, the coefficient of variation of the pressure drop was calculated to further explore the impact of experimental conditions on the flow boiling instabilities in the high aspect ratio micro-channels.

Keywords: flow boiling, instability, pressure drop fluctuation, micro-channel

I. INTRODUCTION

Flow instabilities encountered during two-phase flow boiling were found to cause severe non-uniformities of surface temperature ([1]) and to reduce the boiling heat transfer coefficients ([2]). Flow instabilities would also result in pressure drop fluctuation and lead to high amplitude temperature oscillation ([3,4]). In micro-channel flow boiling, two-phase flow instabilities are even more intense than in conventional channels owing to the confined space for vapour bubble growth. Bergles and Kandlikar [5] also reported reduced critical heat flux (CHF) accompanied with the flow instabilities. These instabilities might be catastrophic if followed by dry-out and could lead to heat exchanger burnout and system failure. Thus, before bringing the micro-channel flow boiling into wider applications, issues of flow instabilities must be addressed to better understand the occurrence of flow instabilities, the impact factors, and the possible options to control and reduce the instabilities.

Various types of instabilities and corresponding unstable flow behaviours in micro-scale flows have been reported in literature. The tendency that instabilities are more severe in micro-channels than macro-channels could be expected, as individual bubbles are more influential on the local pressures in smaller internal volume ([6]). Flow instabilities were proved to cause pressure drop fluctuations and to deteriorate the heat transfer during flow boiling in uniformly heated micro-channels ([7]). The pressure fluctuation consequently resulted in fluctuating channel wall temperatures.

So far, there is no theoretical criterion to identify stable and unstable boiling. Several stability criteria were proposed in the previous studies based on experimental data with the aid of visualization as well as synchronous pressure and temperature measurements.

Brutin, *et al.* [8] suggested a stability diagram in term of heat flux versus mass flow rate. The steady state referred to a low pressure drop fluctuation amplitude (< 1kPa) and no characteristic oscillation frequency; while the unsteady state was defined by a high fluctuation amplitude (>1kPa) and a characteristic frequency of a peak amplitude-to-noise amplitude ratio higher than 20. Chang and Pan [9] reported different flow patterns under unstable flows with visual confirmations of forward or reversed slug/annular flows in each channel of the heat sink. Pressure drop oscillation amplitude was suggested to be the index for the occurrence of reverse flow. However, the impact of the reverse flow on the instabilities was not provided in detail. Wang and Cheng [10] suggested the exit vapour quality to be the stable and unstable flow regimes criterion. A critical vapour quality of 0.013 was proposed, above which the flow would turn into unstable.

Unstable flow boiling was also classified into two sub-types according to the oscillation period length. Wang *et al*. [11] identified two unstable flow regimes with long-period oscillation (more than 1 s) and short-period oscillation (less than 0.1 s). Based on the visualization results, it was found that the long-period oscillation unstable flow boiling was induced by the transition from annular flow to mist flow. On the other hand, the short-period oscillation unstable flow boiling was a result of vapour expansion. Efforts have been made to find the influence factors on two-phase flow stability. Effects of inlet conditions on two-phase flow pressure fluctuation amplitude and frequency were discussed by [12], revealing a much smaller fluctuation amplitude at a constant inlet liquid velocity than a constant outlet velocity. In addition, the differences between single channel and parallel channels were evidenced. Ding, *et al.* [13] believed that less upstream compressible volume was required in single channel to initiate pressure-drop instability than in parallel channels. Therefore it was easier to detect the flow instability in single micro-channel. Wang, *et al.* [11] emphasized the much longer temperature fluctuation in single channel than in parallel channels which they believed was a result of the significant flow interaction from neighboring parallel channels. Singh, *et al.* [14] pointed out that for both single channel and multi-channel conditions, averaged pressure drop increased with increasing heat flux for a constant mass flux. It was noticed that the fluctuations in parallel channels were not as periodic as in single channel. Nevertheless, higher pressure drop was found in parallel channels, reinforcing the explanation that fluctuation was caused by periodic bubble formation and departure.

Recently published investigations revealed some new flow instability characteristics. A fluctuation minimum with increasing heat flux was firstly reported by [14]. Additionally, the transitions between flow patterns showed different stabilities depending on the heat flux and

mass flux ([15]). Stable alternation was observed at high or very high heat flux and mass flux conditions while oscillating flow with instabilities were captured at low heat flux and mass flux.

Accordingly, two-phase pressure drop fluctuation can be significantly affected by the employed experimental conditions, the tendency of which needs to be explored by further experimental investigations. In the present study, flow instabilities are analyzed based on the two-phase pressure drop and channel surface temperature fluctuations as well as the synchronous visualization results. Effects of heat flux, mass flux and the microchannel geometry on flow boiling pressure drop oscillation are discussed.

II. EXPERIMENTAL SETUPS

The experimental setups used in the present investigation of two-phase flow instabilities can be found in [16]. All the experiments were conducted at atmospheric pressure. Degassed FC-72 was used as the working liquid. Ambient temperature was maintained at 25°C. The inlet and outlet pressures of the micro-channel test section were acquired via a National Instruments® Data Acquisition card at a predetermined acquisition frequency of 200 Hz. The offset pressures resulted from the background noises were recorded prior to each test when the channel was filled with stagnant working fluid. Then the offset pressures were subtracted from the acquired raw data. Meanwhile, the boiling process was synchronously visualized by the high speed camera and analyzed with the Image Pro.® software. Pressure drop fluctuation was associated with the synchronous visualization results to show liquid-vapour behaviours in time domain. Subsequently, Fast Fourier Transformation (FFT) was performed on the pressure drop results in Origin® software to assess the pressure drop fluctuation in frequency domain. In addition, an Infrared camera Thermovision® 900 (maximum speed: 7 fps; accuracy: ± 1%) was utilized to obtain the temperature profile along the channel outer surface. Table 1 lists the test conditions of the present study.

Table 1. Experimental conditions in the present study

channel d_h [μm]	Heat flux q [kW·m^{-2}]	Mass flux G [kg·m^{-2}·s^{-1}]
571, 762, 1454	0 – 18.31	11.2, 22.4 and 44.8

III. DATA REDUCTION

Efforts have been made to reasonably obtain reliable averaged pressure data from the temporal inlet and outlet pressure measurements. In order to assess the sensitivity of the averaged pressure results to the averaging method used, we averaged the temporal pressure data using three methods. Firstly, arithmetic mean ($\overline{P} = \frac{1}{n}\sum_{i=1}^{n} P_i$) was applied on the entire

pressure data group. The average pressure could also be computed as $\overline{P} = \frac{1}{\tau}\int_0^t P(t)dt$, where τ is the time during which the data group is obtained (usually lasts 240-400 seconds). In the present study, the pressure fluctuation period is found to be less than 20 second. Since τ is much higher than the fluctuation period, the influence of τ on the mean pressure can be neglected. In order to evaluate the integration, two numerical methods, *Simpson's Rule* and *Newton-Cotes Formula* were used to solve the integration. The averaged pressure data with Simpson's Rule and Newton-Cotes Rule were compared with that of the arithmetic mean results. As can be seen in Table 2, the differences among these three methods are insignificant. Besides, arithmetic mean is the simplest and least time-consuming among the three. Thus, arithmetic mean method is chosen as the pressure averaging method in the present study.

Table 2. Comparison of the pressure data averaging methods

Method	**Maximum deviation from the results calculated in Method 1**
1. Arithmetic mean	0 %
2. Simpson's Rule	1.75 %
3. Newton-Cotes	0.61 %

IV. RESULTS AND DISCUSSION

1. Two-phase pressure and synchronous visualization results

After boiling incipient, the two-phase pressures were found to be fluctuating with high amplitude. The fluctuations were believed to be triggered by the liquid-vapour two-phase flow according to the comparison with single phase pressure measurements. Transient pressure measurements accompanied with the visualization results are exhibited as follows to demonstrate the different fluctuation types and the corresponding two-phase flow behaviors at various mass fluxes and heat fluxes.

First of all, low mass flux and low heat flux conditions are employed. Fig.1 (b) shows the time interval between two pressure oscillation peaks in Fig.1 (a). The results were obtained in the channel with d_h = 571 μm at G = 11.2 kg·m^{-2}·s^{-1} and q = 2.86 kW·m^{-2}. Two types of fluctuations are identified. The one with longer period (~ 14.33 s) has higher amplitude. This low-frequency high-amplitude fluctuation is considered as the major fluctuation due to the reverse flow. According to the observation, the low-frequency high-amplitude fluctuation is caused by the rapid vapor expansion and recoiling after nucleation. Fig.2 shows a series of the corresponding high speed camera sequences. The recoiling can be explained based on the force analysis on the liquid vapour interface. As the evaporation proceeds, certain amount of liquid turns into vapour phase. The interface rapidly propagates toward both downstream and upstream. As a result of the difference between the liquid and vapour densities, the vapour moves across the receding interface at a higher velocity than the liquid, resulting in a momentum change at the receding evaporating interface. Therefore, there is a force acting on the interface according to the momentum conservative law. The interface movement is caused by the joint forces on the interface. When the joint force of evaporation momentum change force and the force due to liquid-vapour pressure difference exceed the inertia force of the bulk liquid flow, the reverse flow

commences.

After being filled with vapour, the channel is then re-wetted by upstream fresh liquid, accompanied by a group of pressure oscillations with shorter period (0.20 s – 0.25 s) and lower amplitude. This high-frequency low-amplitude fluctuation can be considered as the minor fluctuation which normally takes place after the major fluctuation. From the visualization results, a cluster of vapour slugs are observed from upstream during re-wetting. The vapour cluster is the consequence of the continuous nucleation on the channel side wall during rewetting, which is caused by the decrease of local pressure. The inlet and outlet pressures are consequently disturbed when the series of vapour collision occurs downstream. As the amount of vapour grows downstream, the vapour pressure is increased. Thus, the upstream vapour slug is suppressed and the length of slug is reduced gradually, the amplitude of the minor fluctuation gets lower till the entire vapour slug cluster passes through and the channel is re-wetted by single phase liquid. Then the major fluctuation occurs again when the next nucleation cycle starts.

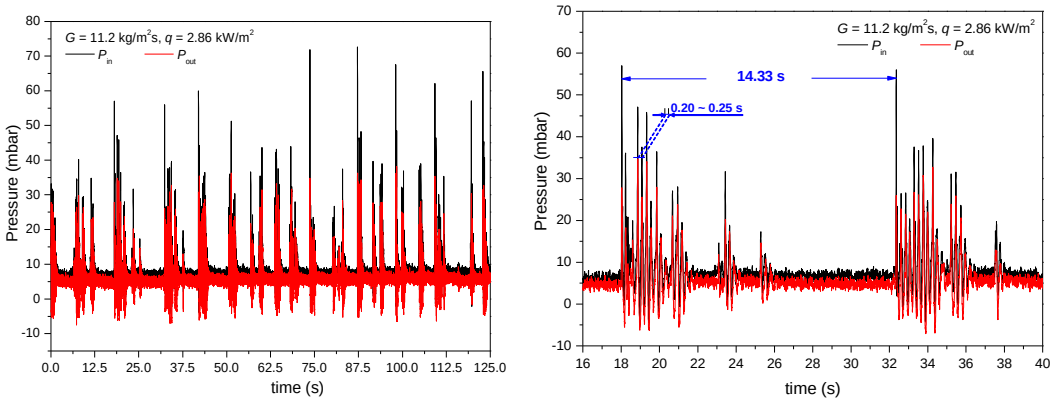

Fig. 1. Inlet and outlet pressures, d_h = 571 μm, G = 11.2 kg·m^{-2}·s^{-1}, q = 2.86 kW·m^{-2}; FC-72

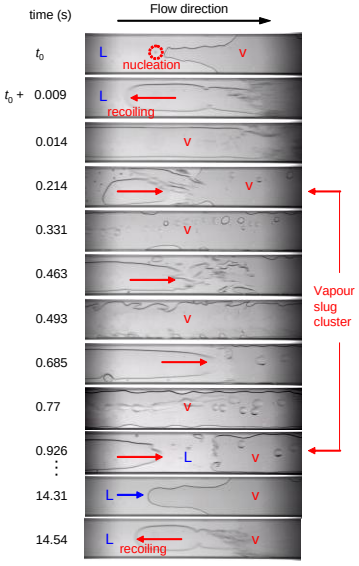

Fig. 2. Visualisation of the flow boiling, d_h = 571 μm, G = 11.2 kg·m^{-2}·s^{-1}, q = 2.86 kW·m^{-2}; FC-72, camera speed: 1500 fps

The frequency of the low-frequency high-amplitude fluctuation is increased as heat flux rises. As shown in Fig.3, heat flux increases to 3.47 kW·m^{-2}. The period of the major fluctuation is about 4.98 s, corresponding to a shorter period of the recoiling-rewetting cycle at a higher heat flux. However, as the heat flux increases, the period of the minor fluctuation is still around 0.20 s – 0.26 s. Similar flow regimes showing the periodic recoiling-vapour slug cluster-rewetting are observed in Fig.4.

Further increase of heat flux results in more intense boiling. In Fig.5, large amount of vapour exists in the channel with high moving speed when heat flux increases to 3.88 kW·m^{-2}. Consequently large numbers of liquid droplets are entrained in the vapour core and are evaporating intensely. Partial dry-out spots on the inner channel surface are observed. At q = 3.88 kW·m^{-2}, the period of the high-frequency low-amplitude fluctuation maintains about 0.22 s. Apparently, the effect of heat flux on the high-frequency low-amplitude fluctuation is marginal.

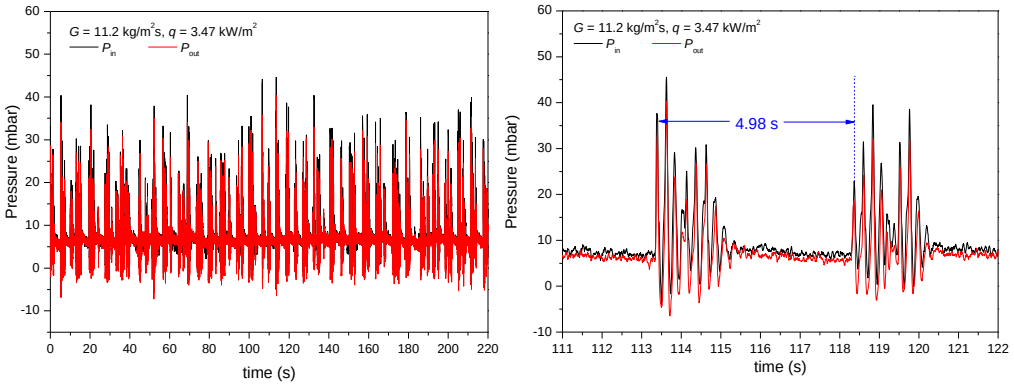

Fig. 3. Inlet and outlet pressures, d_h = 571 μm, G = 11.2 kg·m^{-2}·s^{-1}, q = 3.47 kW·m^{-2}; FC-72

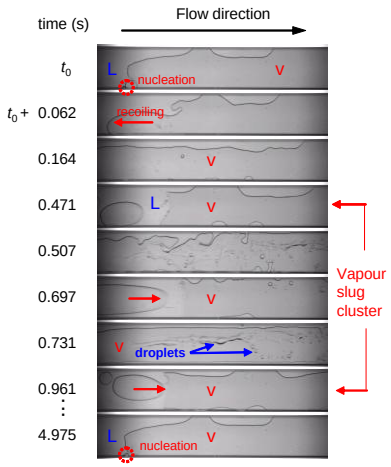

Fig. 4. Visualisation of the flow boiling, d_h = 571 μm, G = 11.2 kg·m^{-2}·s^{-1}, q = 3.47 kW·m^{-2}; FC-72, camera speed: 2000 fps

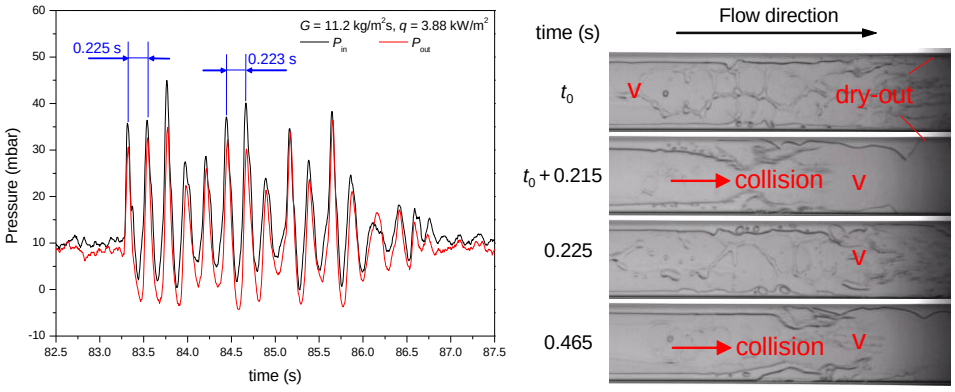

(a) **(b)**

Fig. 5. (a) Minor fluctuations of the inlet and outlet pressures, d_h = 571 µm, G = 11.2 kg·m^{-2}·s^{-1}, q = 3.88 kW·m^{-2}. (b) Corresponding visualisation of vapour collisions; FC-72, camera speed: 2500 fps

Mass flux is found to be influential on the pressure fluctuation. Compared with the results obtained at G = 22.4 kg·m^{-2}·s^{-1}, only the high-frequency low-amplitude fluctuation is captured at a higher mass flux G = 44.8 kg·m^{-2}·s^{-1}. The fluctuation amplitudes are almost constant (Fig.6), merely with slight decrease when approaching the end of the vapour slug cluster. The period of the minor fluctuation is 0.23 s – 0.24 s. Then the inlet and outlet pressures shortly stay stable when the channel is temporarily re-wetted by single phase liquid prior to the passage of the next vapour slug cluster. The vapour slug cluster passage lasts for a longer time than at the lower mass flux. Fig.7 shows the pressure data in the 571 µm channel at G = 44.8 kg·m^{-2}·s^{-1} and q = 10.31 kW·m^{-2}. Increased heat flux slightly shortened the fluctuation period, which becomes 0.195 s – 0.21 s. This reinforced that the increase of heat flux has minor effect on the high-frequency low-amplitude fluctuation.

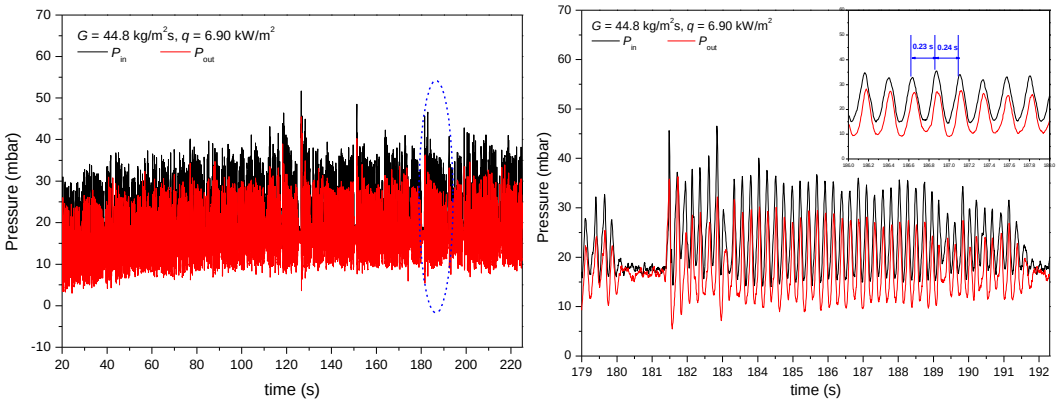

(a) **(b)**

Fig. 6. Inlet and outlet pressures, d_h = 571 µm, G = 44.8 kg·m^{-2}·s^{-1}, q = 6.90 kW·m^{-2}; FC-72

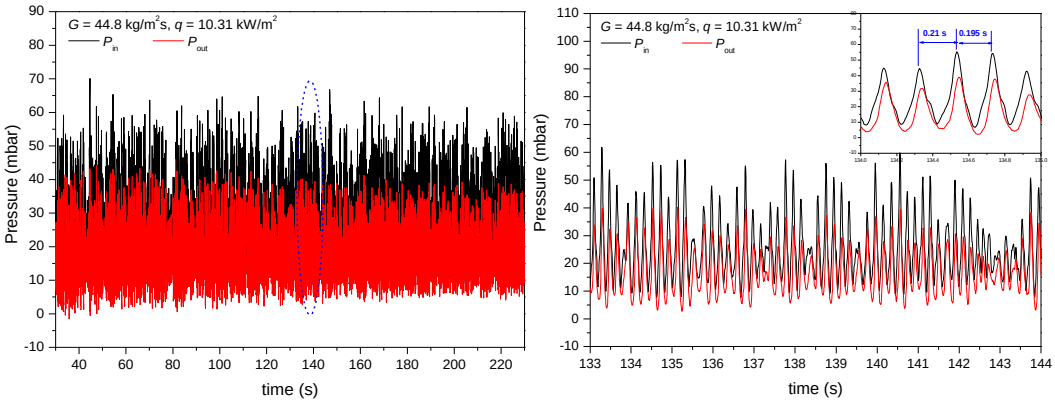

(a) **(b)**

Fig. 7. Inlet and outlet pressures, d_h = 571 μm, G = 44.8 kg·m^{-2}·s^{-1}, q = 10.31 kW·m^{-2}; FC-72

Chaotic boiling ensues when the channel size further increases. The major fluctuation in the 1454 μm channel is still a result of the vapour collision. However, the larger cross-sectional area increases the complexity of the flow field because the increase of channel cross-sectional area provides larger space for thicker liquid film which gives rise to the liquid film nucleation. Fig.8 presents the typical flow regimes and the corresponding P_{in} and P_{out} in the 1454 μm channel at G = 44.8 kg·m^{-2}·s^{-1}. Notable nucleation within the thick liquid film and the fiercely-evaporating droplets entrained in the fast-moving vapour core are observed. According to the visualization results, it is known that while large amount of vapour slugs move rapidly from upstream, liquid films with tiny nucleating bubbles are formed on the channel side-wall. The growth and expansion of these small bubbles will deform the liquid-vapour interface, and will consequently affect the pressures if the interface deformation propagates to the channel inlet and/or outlet.

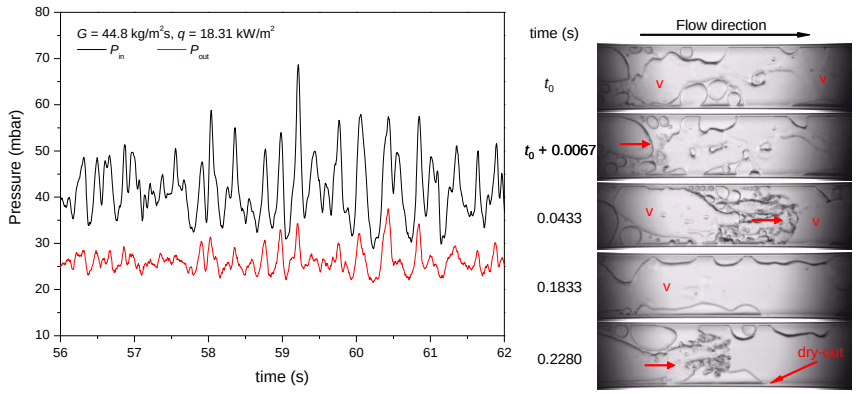

(a) **(b)**

Fig. 8. (a) Inlet and outlet pressures, d_h = 1454 μm, G = 44.8 kg·m^{-2}·s^{-1}, q = 18.31 kW·m^{-2}; FC-72, (b) Corresponding visualisation showing nucleation within liquid film and vapour collision, camera speed: 3000 fps

Furthermore, the liquid vapour movement can be evaluated by using a non-dimensional analyzing tool developed by Kandlikar [17]. The non-dimensional parameter K_1 is selected. K_1 is the ratio of the evapouration momentum force to the inertia force on the liquid-vapour interface ([17]), given by

$$K_1 = \left(\frac{q}{Gh_{fg}}\right)^2 \frac{\rho_l}{\rho_v}$$

Variation of K_1 with microchannel hydraulic diameter for the present experiment at two different mass fluxes is plotted in Fig.9. In the tested ranges, the ranges of K_1 show slight variation in different microchannels at a certain mass flux, which indicates the micro effect of channel hydraulic diameter on the low-frequency high-amplitude fluctuations. However, the values of K_1 at G = 11.2 kg·m^{-2}·s^{-1} is notably higher than those at G = 44.8 kg·m^{-2}·s^{-1}. The difference is mainly shown according to the reverse flow. Thus, at G = 11.2 kg·m^{-2}·s^{-1}, interface movement is mainly dominated by the evaporation momentum force. At a higher mass flux, the inertia force of the bulk liquid is more influential and retards the rapid reversal expansion of the vapour. Instead, vapour collision takes place at a relatively high frequency. This explains why the low frequency high amplitude fluctuation is not captured at G = 44.8 kg·m^{-2}·s^{-1}.

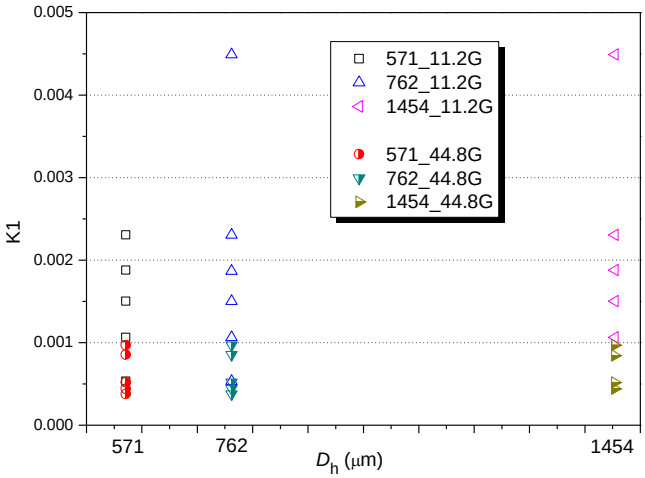

Fig. 9 Ranges of K_1 in the present study

2. Analysis of two-phase pressure drop

The obtained pressure drop data are analyzed to discuss the effects of heat flux, mass flux and the channel dimension on the fluctuation frequency and amplitude. First of all, the averaged pressure drop (see averaging method in Data reduction section) is plotted against q in Fig.10 (a). All the pressure drop data acquired in the micro-channels at G = 11.2 kg·m^{-2}·s^{-1}, 22.4 kg·m^{-2}·s^{-1} and 44.8 kg·m^{-2}·s^{-1} are included. For each flow rate, the applied heat fluxes are limited in certain ranges, which are restricted by the onset of boiling and the critical heat flux. Generally, the averaged pressure drop increases with increasing heat flux. Meanwhile, the pressure drop becomes higher as the mass flux increases from 11.2 kg·m^{-2}·s^{-1} to 44.8 kg·m^{-2}·s^{-1}. This is as expected because the higher averaged pressure drop is induced by the increased flow resistance at higher mass flux.

Furthermore, interesting trends can be captured when plot ΔP as a function of q/G in Fig.10 (b). It can be seen that the impact of q/G on ΔP evidently depends on the applied mass

flux. Generally, ΔP scatters can be linearly fitted. As the ratio of q/G increases, ΔP maintains a relatively constant trend when G = 11.2 kg·m^{-2}·s^{-1}; when the mass flux rises to 22.4 kg·m^{-2}·s^{-1} and 44.8 kg·m^{-2}·s^{-1}, the scope of the fitting line increases as G becomes higher. Accordingly, the dominant effect of mass flux on two-phase flow boiling pressure drop is highlighted.

It is worth mentioning that the pressure drop results presented in this section are the total pressure drop measurements during two-phase flow. Thus the pressure drop consists of the pressure drop due to wall friction, pressure drop due to sudden contraction and expansion at the micro-channel connections and the pressure drop due to acceleration which depends on the averaged void fraction and density change ([18]). According to [18], the contraction and acceleration pressure drops only take small parts of the total pressure drop in circular micro-channels (0.05% – 9% and 0% – 4.5% respectively). Thus the main contribution of the pressure drop is from the friction pressure drop during the flow. However, in the present study, large amount of vapour exists in the high aspect ratio channel during the slug-annular flow and/or annular flow. Thus the accelerational pressure drop is expected to be more considerable than that in the regular channel geometries.

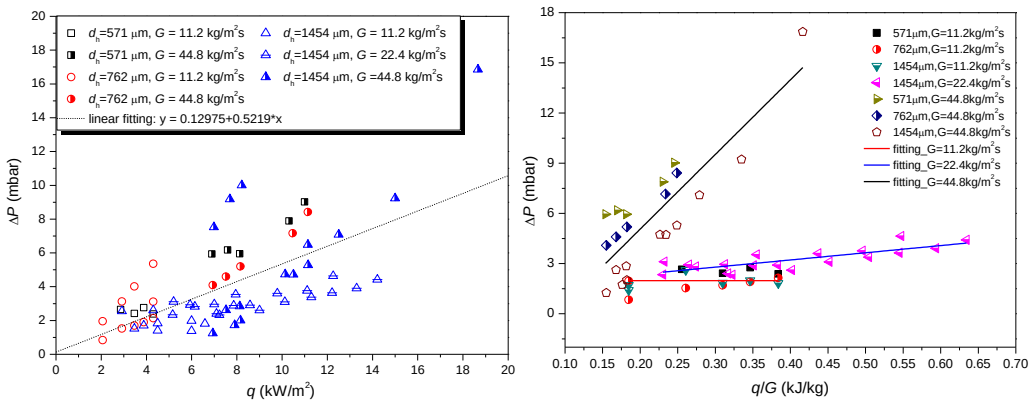

(a) (b)

Fig. 10. Average pressure drop in the three micro-channels at G = 11.2 kg·m^{-2}·s^{-1}, 22.4 kg·m^{-2}·s^{-1} and 44.8 kg·m^{-2}·s^{-1}; FC-72; (a) versus applied heat flux, (b) versus q/G

Then, Origin® software was used to transform the time domain pressure drop data into frequency domain data for signal analysis. Frequency spectrums of the pressure drop at each tested heat fluxes and mass fluxes were obtained. Fig.11 gives the frequency spectrums of the pressure drop signals during single phase and two-phase flows. Apparently, the differences between single phase and two-phase pressure drop frequency spectrums are distinguishable. The frequencies with remarkably higher amplitude are considered to be the consequence of two-phase flow instabilities. Frequencies with considerable amplitude are mostly lower than 10 Hz. Therefore the remaining part of frequency distribution is not shown in the plots, Fig. 11. For two-phase pressure drop, the frequencies with the highest amplitudes were marked as the dominant frequencies. The amplitudes of the dominating frequencies at each heat flux are summarized in Table 3. As can be seen in Fig.11 and Table 3, there are mainly two types of fluctuations, the frequencies of which are in the order of 0.1 Hz and 1 Hz, corresponding to low-frequency fluctuation and high-frequency fluctuation. This is consistent with the previous

analysis. The low-frequency high-amplitude fluctuations and high-frequency low-amplitude fluctuations were also captured during flow boiling in silicon multi-micro-channels by [4]. The low-frequency high-amplitude fluctuations were considered to be the result of the alternation between liquid, two-phase and vapour flow, while the high-frequency low-amplitude fluctuations were mainly caused by the bubble growth between the two successive "refill". The present study managed to obtain simultaneous measurements of channel wall temperature in conjunction with local flow visualization and pressure drop measurements across a high aspect ratio micro-channel with the aid of infrared camera and transparent heating technique. Data acquisition synchronization and the novel transparent heating technique are helpful in revealing the complex internal flow boiling in micro-channels and exploring further the mechanisms for these instabilities.

The occurrence of each type of fluctuation is sensitive to the thermal and flow conditions. For lower mass flux (G = 11.2 kg·m^{-2}·s^{-1}), the low-frequency pressure drop fluctuation shows increasing frequency as the heat flux increases, the corresponding amplitude is also generally increasing. As listed in Table 3, within the same heat flux range, the low-frequency amplitudes increase from 0.79 to 1.36 in the 571 μm channel and from 1.72 to 3.08 in the 762 μm channel. The increase of fluctuation amplitude is less obvious in the d_h = 1454 μm channel, which stays around 0.42 – 0.49, indicating that for a given mass flux, the pressure drop fluctuation amplitudes of low frequencies are more sensitive to heat flux in smaller micro-channels. For the high-frequency fluctuation, the amplitude is relatively lower than those of the low-frequency at a certain heat flux and mass flux. Besides, the amplitudes of high-frequency fluctuations are only slightly increased by increasing heat flux. However, the two types of fluctuations do not occur in every test. Take the 762 μm channel for instance, f = 4.48 Hz and 4.52 Hz are detected only once at q = 3.87 kW·m^{-2} and 4.30 kW·m^{-2} and G = 11.2 kg·m^{-2}·s^{-1}, while in the 1454 μm channel, the low-frequency fluctuation only occurs twice. Visualization reveals that the pressure drop fluctuation is strongly related to the local flow conditions and liquid-vapour distribution, which could be different even at the same heat flux and mass flux. The role of the channel dimension must be highlighted. The low-frequency fluctuations are more likely to take place in smaller channels.

It can be found in Table 3 that at G = 44.8 kg·m^{-2}·s^{-1}, pressure drop fluctuates at a relatively steady frequency and amplitude ranges. Therefore it can be concluded that the increase of mass flux could suppress reverse flow. This is as expected because the reverse flow is caused by insufficient upstream-liquid energy to overcome the downstream high pressure resistance ([14,19]). The liquid could only re-enter the channel when the upstream liquid has enough potential to provide a sufficiently high pressure. At a higher mass flux, upstream liquid has higher potential to suppress the reverse flow.

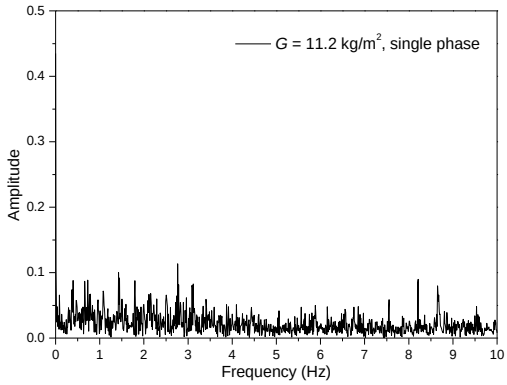

(a)

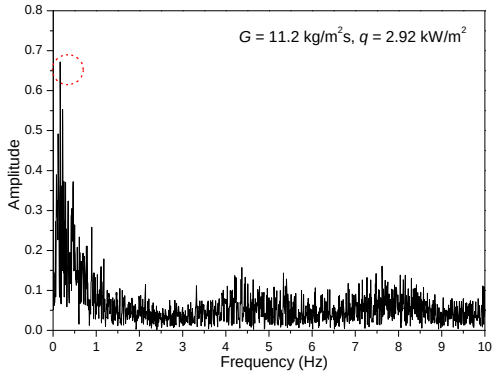

(b)

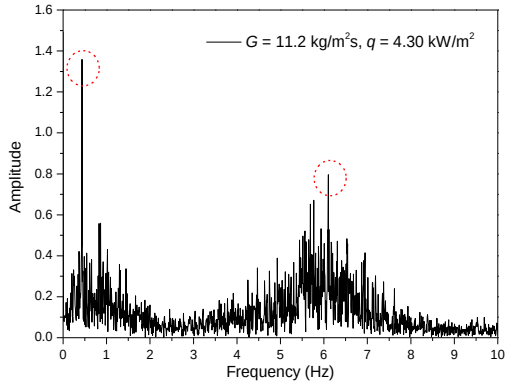

(c)

Fig. 11. Pressure drop fluctuation frequency spectrums; d_h = 571 μm G = 11.2 kg·m^{-2}·s^{-1}; FC-72; (a) single phase flow, (b) two-phase flow, q = 2.92 kW·m^{-2}, (c) two-phase flow, q = 4.30 kW·m^{-2}

Table 3. The dominant frequencies of pressure drop fluctuation in the three micro-channels under ranges of heat fluxes at two mass fluxes; FC-72

d_h (μm)	G = 11.2 kg·m^{-2}·s^{-1}			G = 44.8 kg·m^{-2}·s^{-1}		
	q (kW·m^{-2})	frequency (Hz)	amplitude	q (kW·m^{-2})	frequency (Hz)	amplitude
571	2.07	0.27	0.79	6.94	0.80, 4.82	0.53, 0.60
	2.92	0.28	0.56	7.52	1.27,	0.55,

		5.47	0.41		4.86	0.35
	3.47	0.41	0.81	8.16	1.32,	0.62,
		5.48	0.55		5.56	0.33
	3.88	0.42,	0.81,	10.47	1.47,	0.66,
		6.06	0.62		5.80	0.77
	4.30	0.44,	1.36,	11.14	6.65	0.65
		6.10	0.80			
	2.07	0.12	1.27	6.94	0.37,	0.43,
					3.02	0.512
	2.92	0.14	2.84	7.52	0.48,	0.46,
					3.86	0.50
762	3.47	0.18,	2.32,	8.16	0.17,	0.56,
		0.66	1.88		4.33	0.59
	3.87	0.41,	2.16,	10.47	0.40	0.43
		4.48	0.312		4.832	0.712
	4.30	0.59,	2.46,	11.14	0.46,	0.679,
		4.25	0.52		5.23	0.86
	6.0	0.58	3.08			
	2.92	1.77,	0.48,	7.52	1.76,	0.51,
		2.75	0.45		3.32	0.36
	3.47	2.36	0.70	8.13	1.80,	0.60,
					2.80	0.81
	3.88	2.60,	0.63,	10.40	1.20,	0.97,
		3.12	0.57		2.40,	1.06,
1454					3.36	0.90
	4.30	0.24,	0.42,	11.14	1.33,	0.96,
		1.95,	0.46,		2.67,	0.94,
		2.29	0.42		3.81	0.92
	6.0	0.54,	0.49,			
		3.18	0.50			

Furthermore, pressure drop fluctuation is evaluated via the coefficient of variation of the pressure drop. The coefficient of variation is a commonly used measurement of variability or diversity, revealing the variation of the data from the average value. It is defined as the ratio of the standard deviation (or root mean square) ΔP_{rms} to the mean value ΔP_{avg}. A high coefficient of variation indicates that the data are scattered over a wide range of values ([20]). It is worth mentioning that this analysis method was also previously used by [14].

The standard deviation of the pressure drop ΔP_{rms} is calculates as:

$$\Delta P_{\text{rms}} = \sqrt{\sum_{i=1}^{N} (\Delta P_i - \Delta P_{\text{avg}})^2 / N} \quad (1)$$

where ΔP_i is the transient pressure drop, ΔP_{avg} is the arithmetically-averaged value of the pressure drop data string, and N is the number of the data points.

The coefficients of variation $\Delta P_{rms} / \Delta P_{avg}$ in three channels are plotted against the ratio of q/G in Fig.12 at two different mass fluxes. When G = 11.2 kg·m^{-2}·s^{-1}, $\Delta P_{rms} / \Delta P_{avg}$ increases with increasing q/G. When G = 44.8 kg·m^{-2}·s^{-1}, however, decreasing trend of $\Delta P_{rms} / \Delta P_{avg}$ is found when q/G increases, indicating the dominance of mass flux on pressure drop diversity.

Fig.12 also emphasizes the effect of channel hydraulic diameter. At G = 44.8 kg·m^{-2}·s^{-1}, $\Delta P_{rms} / \Delta P_{avg}$ increases as the channel hydraulic diameter increases from 571 μm to 1454 μm. However, at G = 11.2 kg·m^{-2}·s^{-1} the increase of $\Delta P_{rms} / \Delta P_{avg}$ is more pronounced in low q/G region, beyond which the data in three channels merge together. Accordingly, the impact of channel size on flow instability is more profound at higher mass flux. Nevertheless, the experimental range was limited by the heat input power and pumping capacity. Further investigations with wider experimental ranges are essential to explore the influences on the pressure fluctuation.

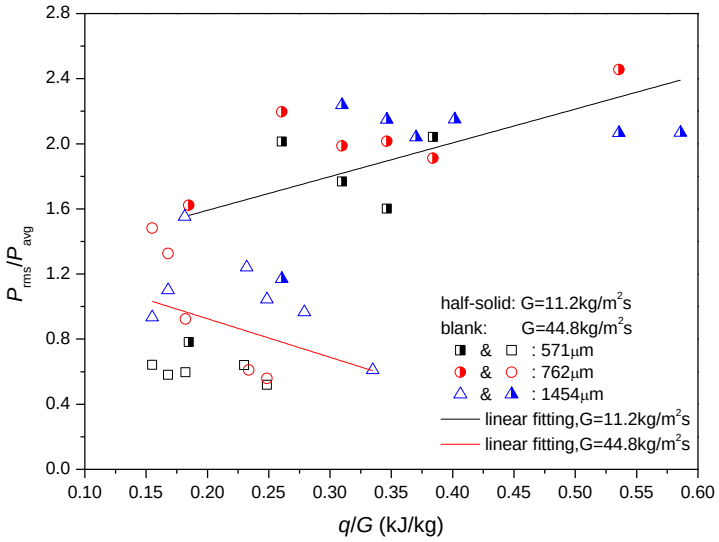

Fig. 12. Coefficients of variation obtained at ranges of heat fluxes and two mass fluxes in three microchannels; FC-72.

3. Channel wall temperature fluctuations

Channel wall temperature is found to be fluctuating after boiling started. The deposition of the coating on the micro-channel exterior wall was uniform, hence the applied heat flux was uniform. So the temperature fluctuations captured at the wall can only caused by the two-phase flow occurring inside the micro-channel. The periodic temperature fluctuation is evidently related to the liquid-vapour distribution within the channel and is a consequence of the periodic reverse and rewetting flow. Fig.14 is the channel wall temperature map during the reverse and rewetting flow. The 3-dimensional coordinates provide a more quantitative perspective of the temperature profiles. This corresponds to the low-frequency high-amplitude fluctuation. As the liquid temperature gradually increases, vapour firstly appears near the

channel exit. Then the rapid vapour expansion triggers the reverse flow with the recoiling propagating towards upstream. At the locations occupied by vapour phase, the liquid layer beneath the vapour bubble keeps on evaporating and partial dry-out appears before being replenished by fresh liquid. Therefore the channel wall temperatures at these dry-out spots jump to a much higher level. As the vapour expands, the high-temperature spot also expands till the upstream liquid has sufficient potential to overcome the high vapour pressure and to rewet the channel surface. Consequently channel surface is cooled down by the liquid rewetting.

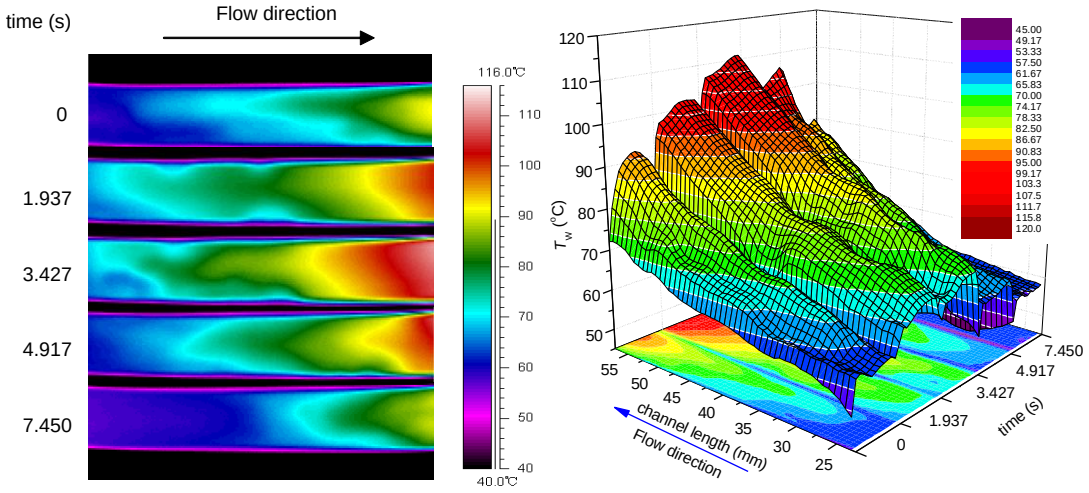

Fig. 13. Infrared sequences of channel surface temperatures and the 3-dimensional plot; d_h = 571 μm, G = 11.2 kg·m^{-2}·s^{-1}, q = 2.07 kW·m^{-2}; FC-72

When the high-frequency low-amplitude fluctuations occur in the flow, the channel surface temperature distributes differently. As can be seen from Fig.15, a higher heat flux q = 4.30 kW·m^{-2} is applied on the channel surface, temperature still gradually grows along the channel stream-wise direction. Very high T_w is achieved near the channel exit where large amount of vapour exists. The temperature fluctuation between frames is not as remarkable as in Fig.15. Since the reverse flow is largely suppressed as mass flux increases, the vapour-occupied portion in the channel constantly exists. In this circumstance, the high temperature area should be monitored with special attention because the constantly high channel wall temperature could easily result in surface destruction.

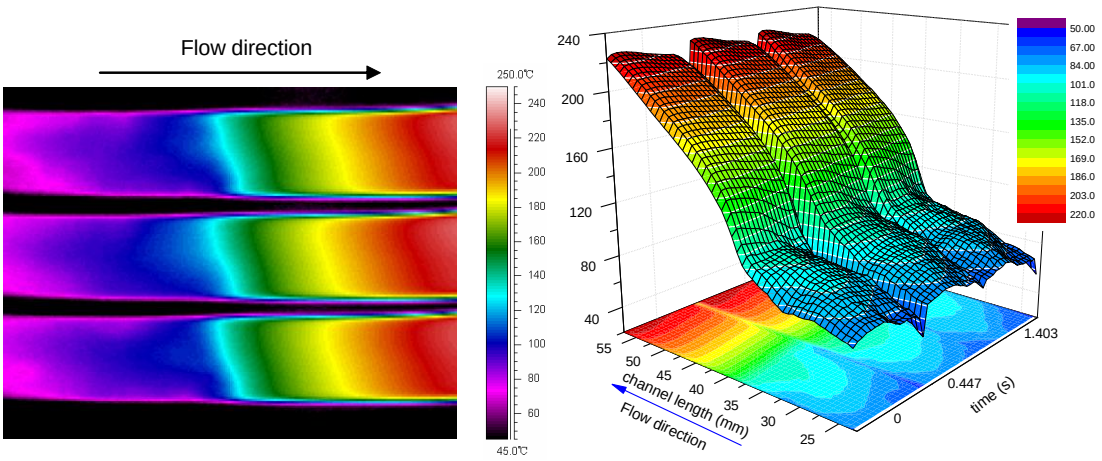

Fig. 14. Infrared sequences of channel surface temperatures and the 3-dimensional plot; d_h = 571 μm, G = 11.2 kg·m^{-2}·s^{-1}, q = 4.30 kW·m^{-2}; FC-72

V. CONCLUSIONS

Two-phase flow instabilities in single high-aspect-ratio rectangular micro-channels were experimentally investigated. Degassed FC-72 was tested in micro-channels with a hydraulic diameters of 571 μm, 762 μm and 1454 μm at liquid mass fluxes of 11.2 kg·m^{-2}·s^{-1}, 22.4 kg·m^{-2}·s^{-1} and 44.8 kg·m^{-2}·s^{-1} and heat fluxes of 0-18.31 kW·m^{-2}. The pressure drop across the micro-channels was recorded. Synchronous visualization results and microchannel surface temperature profiles were also obtained. In light of the present study, the following conclusions can be drawn.

- Low-frequency fluctuations and high-frequency fluctuations are identified. Based on the visualization results, the low-frequency high-amplitude fluctuation is the major fluctuation mode at lower mass flux, resulting from the periodic reverse and rewetting flow. The interface movement is caused by the joint forces on the interface. When the joint force of evaporation momentum change force and the force due to liquid-vapour pressure difference exceed the inertia force due to bulk liquid flow, the reverse flow commences.
- The frequency of the low-frequency high-amplitude fluctuation is increased as heat flux rises. However, the low-frequency oscillation is largely suppressed by increasing mass flux.
- The high-frequency low-amplitude fluctuation is caused by the vapour slug cluster passage during the rewetting flow and the vapour collision at downstream. Effect of heat flux on the high-frequency low-amplitude fluctuation is insignificant. Nevertheless, mass flux is found to be remarkably influential on the pressure fluctuation. The high-frequency low-amplitude fluctuation is the minor fluctuation mode at lower mass flux, but becomes dominant at higher mass fluxes.
- The non-dimensional analyzing tool developed by Kandlikar [17,21] is used to better understand the liquid vapour interface movement. It is found that at G = 11.2 kg·m^{-2}·s^{-1}, interface movement is mainly dominated by the evaporation momentum

force. At a higher mass flux, the inertia force of the bulk liquid is more influential and retards the rapid reversal expansion of the vapour.

- Channel surface temperature is fluctuating owing to the periodic reversal and rewetting flow and the consequent local partial dry-out. The high temperature area should be monitored with special attention because the constantly high channel wall temperature could easily result in surface damage.
- Micro-channel hydraulic diameter also has some impact on the pressure drop fluctuation. The pressure drop data is more chaotic as the channel size increases. Based on the FFT computation, it is found that the pressure drop fluctuation amplitudes of low frequencies are more sensitive to heat flux in smaller micro-channels for a given mass flux.
- Moreover, the averaged pressure drop increases with increasing q/G, the scatters of which are linearly fitted and the scope of the fitting line increases as G becomes higher. The coefficient of variation of the pressure drop data $\Delta P_{rms} / \Delta P_{avg}$ is calculated as a measurement of the pressure drop diversity. For G = 11.2 kg·m^{-2}·s^{-1}, $\Delta P_{rms} / \Delta P_{avg}$ increases with increasing q/G, the increasing rate gets higher as the channel size reduces. However, at G = 44.8 kg·m^{-2}·s^{-1}, $\Delta P_{rms} / \Delta P_{avg}$ decreases with q/G, but is an increasing function of the channel hydraulic diameter.

ACKNOWLEDGEMENTS

This research was supported by the UK Engineering and Physical Sciences Research Council (EPSRC). The experiments were conducted at the University of Edinburgh during the first author's PhD study. The authors would also like to acknowledge the support from the China Scholarship Council (CSC) and the Research Project of National University of Defense Technology (JC12-01-10).

NOMENCLATURE

d_h	hydraulic diameter (m)
f	Frequency (Hz)
G	mass flux (kg·m^{-2}·s^{-1})
P	pressure (Pa)
ΔP_{avg}	arithmetic mean pressure drop
ΔP_{rms}	root mean square of pressure drop
q	heat flux (kW·m^{-2})
T	temperature (°C)
X_k	amplitude

REFERENCES

[1]. G. Hetsroni, A. Mosyak,Z. Segal, *Nonuniform temperature distribution in electronic devices cooled by flow in parallel microchannels*. Components and Packaging Technologies, IEEE Transactions on, 2001.24(1):16-23.

[2]. W. Qu,I. Mudawar, *Measurement and prediction of pressure drop in two-phase micro-channel heat sinks*. International Journal of Heat and Mass Transfer, 2003.46(15):2737-2753.

[3]. J. Barber, K. Sefiane, D. Brutin,L. Tadrist, *Hydrodynamics and heat transfer during flow boiling instabilities in a single microchannel*. Applied Thermal Engineering, 2009.29(7):1299-1308.

[4]. D. Bogojevic, K. Sefiane, A.J. Walton, H. Lin,G. Cummins, *Two-phase flow instabilities in a silicon microchannels heat sink*. International Journal of Heat and Fluid Flow, 2009.30(5):854-867.

[5]. A.E. Bergles,S.G. Kandlikar, *On the Nature of Critical Heat Flux in Microchannels*. ASME Conference Proceedings, 2003.2003(37149):701-707.

[6]. L. Zhang, E.N. Wang, K.E. Goodson,T.W. Kenny, *Phase change phenomena in silicon microchannels*. International Journal of Heat and Mass Transfer, 2005.48(8):1572-1582.

[7]. G. Hetsroni, A. Mosyak, Z. Segal,G. Ziskind, *A uniform temperature heat sink for cooling of electronic devices*. International Journal of Heat and Mass Transfer, 2002.45(16):3275-3286.

[8]. D. Brutin, F. Topin,L. Tadrist, *Experimental study of unsteady convective boiling in heated minichannels*. International Journal of Heat and Mass Transfer, 2003.46(16):2957-2965.

[9]. K.H. Chang,C. Pan, *Two-phase flow instability for boiling in a microchannel heat sink*. International Journal of Heat and Mass Transfer, 2007.50(11-12):2078-2088.

[10]. G. Wang,P. Cheng, *An experimental study of flow boiling instability in a single microchannel*. International Communications in Heat and Mass Transfer, 2008.35(10):1229-1234.

[11]. G. Wang, P. Cheng,H. Wu, *Unstable and stable flow boiling in parallel microchannels and in a single microchannel*. International Journal of Heat and Mass Transfer, 2007.50(21-22):4297-4310.

[12]. D. Brutin,L. Tadrist, *Pressure drop and heat transfer analysis of flow boiling in a minichannel: influence of the inlet condition on two-phase flow stability*. International Journal of Heat and Mass Transfer, 2004.47(10-11):2365-2377.

[13]. Y. Ding, S. Kakaç,X.J. Chen, *Dynamic instabilities of boiling two-phase flow in a single horizontal channel*. Experimental Thermal and Fluid Science, 1995.11(4):327-342.

[14]. S.G. Singh, R.R. Bhide, S.P. Duttagupta, B.P. Puranik,A. Agrawal, *Two-Phase Flow Pressure Drop Characteristics in Trapezoidal Silicon Microchannels*. Components and Packaging Technologies, IEEE Transactions on, 2009.32(4):887-900.

[15]. G.P. Celata, S.K. Saha, G. Zummo,D. Dossevi, *Heat transfer characteristics of flow boiling in a single horizontal microchannel*. International Journal of Thermal Sciences, 2010.49(7):1086-1094.

[16]. Y. WANG,K. Sefiane, *Effects of heat flux, vapour quality, channel hydraulic diameter on flow boiling heat transfer in variable aspect ratio micro-channels using transparent heating*. International Journal of Heat and Mass Transfer, 2012.55(9–10):2235-2243.

[17]. S.G. Kandlikar, *Heat Transfer Mechanisms During Flow Boiling in Microchannels*. Journal of Heat Transfer, 2004.126(1):8-16.

[18]. A. Kawahara, P.M.Y. Chung,M. Kawaji, *Investigation of two-phase flow pattern, void fraction and pressure drop in a microchannel*. International Journal of Multiphase Flow, 2002.28(9):1411-1435.

[19]. Y. Wang, K. Sefiane,R. Bennacer, *Investigation of boiling and bubble confinement in a high aspect ratio micro-channel*. Applied Thermal Engineering, 2011.31(5):610-618.

[20]. J.D. Schwarzkopf, S.G. Penoncello,P. Dutta, *Enhanced boiling heat transfer in mesochannels*. International Journal of Heat and Mass Transfer, 2009.52(25-26):5802-5813.

[21]. X.F. Peng,B.X. Wang, *Forced convection and flow boiling heat transfer for liquid flowing through microchannels*. International Journal of Heat and Mass Transfer, 1993.36(14):3421-3427.